Energy Efficiency of the Carbonate Hydroxyapatite Nanoparticle Synthesis Using Microwave Heating Treatment and Its Effect on Material Characteristics

Saifuddin Aziz[1], Harno Dwi Pranowo[1*], Ika Dewi Ana[2,3], and Yusril Yusuf[3,4]

[1]*Department of Chemistry, Faculty of Mathematics and Natural Sciences, Universitas Gadjah Mada, Sekip Utara, Yogyakarta 55281, Indonesia*

[2]*Department of Dental Biomedical Science, Faculty of Dentistry, Universitas Gadjah Mada, Yogyakarta 55281, Indonesia*

[3]*Research Collaboration Center for Biomedical Scaffolds National Research and Innovation Agency of Republic of Indonesia (BRIN) and Universitas Gadjah Mada (UGM), Yogyakarta 55281, Indonesia*

[4]*Department of Physics, Faculty of Mathematics and Natural Sciences, Universitas Gadjah Mada, Yogyakarta 55281, Indonesia*

**** Corresponding author:***

email: harnodp@ugm.ac.id

Received: August 20, 2023
Accepted: November 20, 2023

DOI: 10.22146/ijc.88155

Abstract: *This work aimed to study the energy efficiency of the synthesis process of carbonated hydroxyapatite (CHA) nanoparticles using microwave heating treatment and its effect on material characteristics. Microwaves can provide heat quickly, so it is expected to increase the efficiency of CHA synthesis through the heat provided. The CHA nanoparticles were synthesized using precipitation and heated using a microwave oven. The unheated and hydrothermal-heated precipitation methods were also conducted for comparison purposes. The microwave-heated precipitations were done at 270 W for 0.05, 0.10, and 0.15 h, while the hydrothermal-heated precipitations were done at 100 °C for 1, 2, and 3 h. The CHA materials were characterized using an infrared spectrophotometer, X-ray diffractometer, and electron microscope. The X-ray diffractogram and infrared spectra confirmed that the synthesized materials had a hydroxyapatite crystal phase with a CO_3^{2-} functional group in their spectra. Microscopic images revealed that the materials were nanometer-sized grain aggregates. The heat treatment and duration increased the material characteristics, i.e., crystallinity, crystallite, and grain size. The CHA with microwave heat treatment had the highest crystallinity and crystallite size. The electrical energy calculation revealed microwave heating had better energy efficiency than hydrothermal heating.*

Keywords: *carbonate; efficiency; hydroxyapatite; microwave; nanoparticles*

■ INTRODUCTION

Bones are essential in the body to move and protect organs [1]. Although seemingly inert, bone is a dynamic tissue. Bone is continuously resorbed by osteoclast and neoformed by osteoblast cells [2]. Through these cells, bone can regenerate and repair itself. It allows minor bone defects to heal independently without additional treatment. However, if the bone defect exceeds the critical size threshold, the defect cannot be self-repaired. Surgical treatment, such as bone graft placement, is required to treat bone defects [1]. In this point, the use of bone graft is to provide mechanical support and stimulate osteo-regeneration [3].

Hydroxyapatite (HA) is a member of the calcium phosphate mineral family with the chemical formula of $Ca_{10}(PO_4)_6(OH)_2$ [4]. Its bioactivity on bone forming has broadly been applied in the biomedical field, especially in bone regeneration treatment [5]. The calcium and phosphate composition of HA is similar to bone-constituting minerals [6]. In some cases, HA was also used in the formation of doped HA, either to increase its inner antimicrobial properties [7-8] or to enhance its bioresorbability [9].

Although it has a composition like bone mineral, HA does not have an adequate resorption property. It can persist in bone defects for up to 10 years after implantation. The poor resorption properties of HA can cause minor fractures at the bone-material interface or within the material, causing bone deformation [10]. Moreover, compared to the synthetic HA, the bone-constituting mineral is a non-stoichiometric plate-shaped HA with 250 × 500 × 2–4 nm of dimensions [11-12]. The bone-constituting mineral is partially substituted with ions such as carbonate, sodium, magnesium, and potassium [12]. Carbonate ion (CO_3^{2-}) is the most abundant substituent in bone minerals, with a percentage of 2–5% [13-14]. Mimicking bone mineral properties in HA is an effective way to achieve optimal resorption ability similar to bone minerals [10]. Therefore, the nano-carbonate HA (CHA) was developed [15].

The CO_3^{2-} in CHA enhances bioresorbability and osteoconductivity than the HA due to CHA's smaller crystallite size than HA [16-18]. Safarzadeh et al. [18] synthesized CHA with variation in the amount of CO_3^{2-} ion and obtained the size of CHA 94.3, 81.5, 77.2, 72.0, 69.1, and 68.5 nm for 0, 2.01, 2.95, 4.10, 5.05, and 5.25% CO_3^{2-} content. The nanometer-sized properties also provide better cell proliferation and differentiation due to the larger surface area of the nanometer particle than the micrometer [19]. CHA can be synthesized using the HA synthesis method by adding CO_3^{2-} source [20-23].

The synthesis methods include dry, wet, and high-temperature methods. The dry synthesis method included solid-state reaction and mechanochemical. Precipitation, hydrothermal, and hydrolysis are included in the wet synthesis method. Then, the high-temperature methods are combustion and pyrolysis. Solid-state reaction, combustion, and pyrolysis methods involved high temperatures in the synthesis process. The solid-state reaction uses high temperatures to decompose reactants. The high temperature in the combustion method occurs due to the fast exothermic and self-sustaining redox reaction between oxidant and organic fuel. In the pyrolysis method, the high temperature occurs from the used electric furnace. The mechanochemical method does not use high temperatures but requires a long time in the grinding and milling to induce a chemical transformation. HA reformation from $CaHPO_4$ and CaO required 20 h milling process [24]. The long synthesis time also occurs in the wet synthesis method. However, the temperature used in the wet synthesis method is low. The HA material was synthesized using $Ca(NO_3)_2$ by Mobasherpour et al. [25] at 25.0 °C and Correa-Piña et al. [26] at 37.5 °C with an aging time of 48 h.

Among the wet synthesis process, the precipitation method is the most straightforward route [19]. The precipitation method is based on the precipitation of the aqueous solution. This method is suitable for producing HA in large quantities due to the ease of synthesis and the high yield [27]. However, the precipitation method requires 1–7 d of the aging stage to mature the HA crystal [26,28-30]. The microwave energy successfully accelerates the HA precipitation aging process. Hassan et al. [31] reported using a domestic microwave oven to precipitate HA in less than 1 h. Saikiran et al. [32] used microwave heating treatment in their precipitation method to synthesize Zn/Mg and Zn/Mg-F substituted HA in 30 min without any aging stage. The scanning transmission electron microscopy (STEM) analysis affirmed that the synthesized nanopowders are plate-like structures, and the average particle size was 50–60 nm.

Microwaves are magnetic and electrical radiation that can be absorbed by the materials and converted into heat [33]. The absorbed microwaves polarize the molecule with a rapid electrical field reversal, resulting in heat due to intermolecular friction [31]. Unlike the heat from a microwave, conventional electric heaters conduct heat by convection. The container is preheated, and the heat is conducted from the surface of the materials to the core. The heat flow mechanism in microwaves provides the advantages of low energy consumption and reduced processing time [33]. The world energy demand is increasing due to economic growth and chemical industry activity. A renewal of conventional processes is needed to push towards a more sustainable direction.

With low energy consumption, microwave heating was expected to speed up the process and increase the efficiency of CHA synthesis. The CHA materials were

synthesized by precipitation method with microwave heating. The hydrothermal heating and no heating treatment were also applied for comparison purposes. The synthesized materials were characterized using an infrared spectrophotometer, X-ray diffractometer, and electron microscope. The materials were also immersed in the simulated body fluid (SBF) to estimate the bioactivity and chemical stability. The energy efficiency of each method was calculated from the electrical energy consumption.

■ EXPERIMENTAL SECTION

Materials

Calcium nitrate tetrahydrate ($Ca(NO_3)_2{\cdot}4H_2O$), diammonium hydrogen phosphate ($(NH_4)_2HPO_4$), sodium carbonate (Na_2CO_3), and ammonium hydroxide (NH_4OH) were used for the HA and CHA synthesis. The materials used in SBF preparation are sodium chloride (NaCl), sodium hydrogen carbonate ($NaHCO_3$), potassium chloride (KCl), di-potassium hydrogen phosphate trihydrate ($K_2HPO_4{\cdot}3H_2O$), magnesium chloride hexahydrate ($MgCl_2{\cdot}6H_2O$), calcium chloride ($CaCl_2$), sodium sulfate (Na_2SO_4), tris-hydroxymethyl aminomethane ($(HOCH_2)_3CNH_2$), and hydrochloric acid (HCl). All the materials were analytical grade quality and produced by Merck, USA.

Instrumentation

The instruments used in this research aimed at characterizing the materials are Fourier transform-infrared spectrophotometer (FTIR, Shimadzu Prestige 21), X-ray diffractometer (XRD, Bruker D8 ADVANCE ECO), scanning electron microscope (SEM, JEOL JSM-6510LA), and transmission electron microscope (TEM, JEOL JEM-1400). The electrical energy consumption was measured using a kWh meter (SMARTMETER SMI-810 V3).

Procedure

CHA nanoparticles synthesis

The CHA nanoparticles were synthesized with the precipitation method proposed by Mobasherpour et al. [25] and Correa-Piña et al. [26] using $Ca(NO_3)_2$, $(NH_4)_2HPO_4$, and Na_2CO_3 as calcium, phosphate, and carbonate ion sources. The mol ratio of the reactants Ca^{2+}:PO_4^{3-}:OH^- was 1.67:1:1 [23]. As much as 1.771 g of $Ca(NO_3)_2$ was initially diluted in 10 mL H_2O as solution A. Then, solution B was formed by diluting 0.594 g of $(NH_4)_2HPO_4$ and 0.477 g of Na_2CO_3 in 20 mL H_2O. The synthesis process was carried out by mixing the solutions A and B that previously were adjusted to pH 9.85 using NH_4OH. The mixture was stirred for 15 min and then heated using microwave and hydrothermal methods. The microwave heating methods were conducted at 30% power (270 W) for 0.05, 0.10, and 0.15 h. Meanwhile, the hydrothermal heating methods were conducted at 100 °C for 1, 2, and 3 h. For comparison, the unheated CHA materials were also synthesized. The non-heated CHA was synthesized using precipitation with an aging step for 48 h. The synthesized materials were washed using H_2O and dried in a 100 °C oven for 6 h. HA was also synthesized using microwave-assisted precipitation (HA-PMW-39) to compare the carbonate-doped and non-doped HA characters. The materials are named in Table 1.

Material characterization

The synthesized materials were characterized using FTIR to determine the material functional group. The crystal phase identity of the materials was determined using XRD. The diffractogram patterns were fitted and analyzed for their crystalline phase using HighScore Plus software. The SEM and TEM were used for the material morphology analysis. Furthermore, to predict the bioactivity and stability of the material, the HA and CHA materials were immersed in a SBF solution that was made using the Kokubo and Takadama [34] method. As much as 0.1 g of HA and CHA materials were

Table 1. Heat treatment of wet precipitation synthesis process

Heat treatment	Time (h)	Material
Un-heated	-	CHA-P48
Hydrothermal	1	CHA-PHT-101
	2	CHA-PHT-102
	3	CHA-PHT-103
Microwave	0.05	CHA-PMW-33
	0.10	CHA-PMW-36
	0.15	CHA-PMW-39

immersed in SBF solution with pH 7.4 and incubated at 36.5 °C for 30 d. The pH of the SBF solution was measured every 3 d, and the trend was evaluated to estimate the material bioactivity and stability [35-36].

■ RESULTS AND DISCUSSION

The materials were successfully synthesized using the precipitation method with and without thermal treatment. The Ca^{2+}, PO_4^{3-} and CO_3^{2-} ion sources were reacted in the alkaline condition and produced precipitated material. The reaction of the HA formation process is as follows:

$$10Ca(NO_3)_2 + 6(NH_4)_2HPO_4 + 8NH_4OH \rightarrow Ca_{10}(PO_4)_6(OH)_2 + 20NH_4NO_3 + 6H_2O \quad [19]$$

Then, when the carbonate ion is included in the process, the reaction changes to:

$$10Ca(NO_3)_2 + 6(NH_4)_2HPO_4 + xNa_2CO_3 + 8NH_4OH \rightarrow Ca_{10}(PO_4)_{6-x}(CO_3)_x(OH)_2 + 20NH_4OH + xNaOH + xNaHPO_4 + (6-x)H_2O \quad [37]$$

This synthesis process obtained the white-colored materials. Material characterizations were required to determine the identities and properties of the material.

The FTIR recorded vibration of the functional group of the material and were displayed as spectra in Fig. 1. The observed functional group vibrations in Fig. 1 are PO_4^{3-}, CO_3^{2-}, and H_2O. These results have been confirmed using previous research and are presented in Table 2. The broad peak of H_2O at 3411 cm^{-1} shows that the materials have absorbed water molecules on their body. Whereas the 1642 cm^{-1} peak of H_2O results from the vibration of water molecules in the crystal lattice of the material. The CO_3^{2-} peak only appeared on the CHA material spectra due to the addition of the CO_3^{2-} ion in the synthesis process. The PO_4^{3-} peaks in all materials indicate that the resulting materials belong to the calcium phosphate family.

Further characterization is needed to determine the crystalline phase of the material. Characterization using XRD was carried out to determine the crystal phase of the material. The diffractogram of the materials in Fig. 2 was

Table 2. Functional groups and their wavenumber of the synthesized materials

Wavenumber (cm^{-1})		Functional Group
This work	References [21,23,38]	
3411	3700–2800	H_2O
1642	1700–1600	
1489	1550–1450	CO_3^{2-}
1419	1430–1410	
871	890–850	
1072	1120–1020	PO_4^{3-}
956	960	
609	600	
570	500	

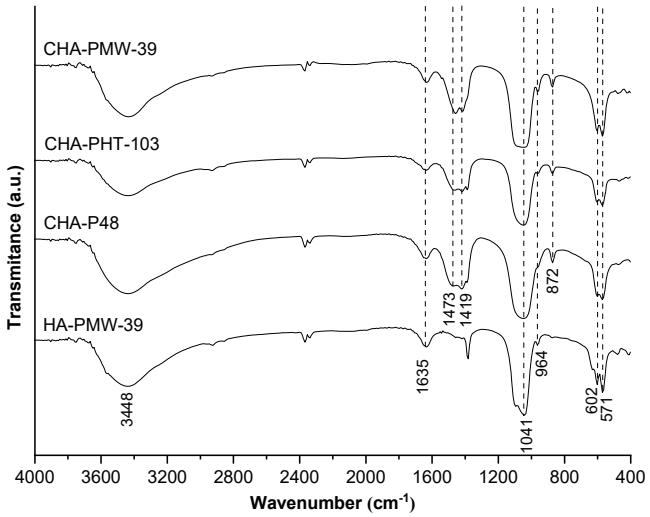

Fig 1. The FTIR spectra of synthesized CHA compared to the HA

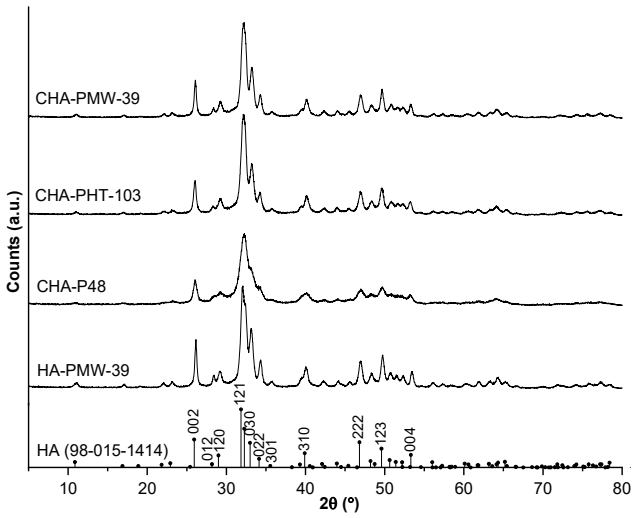

Fig 2. The diffractogram of synthesized CHA compared to the HA diffractogram

searched and matched using HighScore Plus software. Their diffractograms are single-phase only and match that of HA with ICSD 98-05-1414. The XRD and FTIR results revealed that the synthesized materials had HA crystal phases with CO_3^{2-} vibrations. However, the diffractogram did not show any new phase formation, so it was concluded that the synthesized materials were CHA. Moreover, CO_3^{2-} peaks at 871, 1419, and 1489 cm^{-1} in the CHA spectra, which were typical vibrations of B-type CHA, confirmed that the synthesized materials were B-type CHA. This conclusion is also supported by the absence of typical A- and AB-type CHA peaks. The typical CO_3^{2-} vibration of type-A CHA occurs at 877–880, 1500, and 1540–1550 cm^{-1}. Then, the AB-type CHA has a characteristic vibration at 1515 cm^{-1} [23].

The diffractogram in Fig. 2 showed the peaks of diffraction plane 002 (26.04°), 120 (29.26°), 121 (32.12°), 030 (33.20°), 022 (34.12°), 310 (40.13°), 222 (46.90°), and 123 (49.58°). The peak of diffraction plane 002 was used to determine crystallinity and crystallite size. Table 3 shows the result of the crystallinity and crystallite size calculation. Based on the calculation of crystallinity and crystallite size in Table 3, CHA crystallinity and crystallite size were smaller than HA. It showed that incorporating CO_3^{2-} ion into HA material could reduce its crystallinity and crystallite size. The CO_3^{2-} ion substitute PO_4^{3-} ion in the case of B-type CHA. The size of CO_3^{2-} ion is smaller than PO_4^{3-}. The substitution of PO_4^{3-} by CO_3^{2-} in HA material caused defects in the crystal and inhibited crystal growth so a smaller crystallite size crystal was obtained [39].

The CHA materials were synthesized using different heat treatments in this study. Fig. 3 and 4 show the FTIR spectra and XRD of the CHA material with variations in the heat treatment method. The FTIR spectra in Fig. 3 show that the CHA materials have similar spectra. It can be concluded that the difference in heat treatment does not affect the functional group composition of the CHA material. The material diffractogram in Fig. 4 shows that the peaks of each CHA material are slightly different. The number of peaks on the diffractogram is the same, but the peak heights look different. The difference in peak height indicates the difference in crystallinity of the CHA material. The crystallinity and crystallite size of the CHA material with heat treatment variation are shown in Table 3. Comparing the crystallinity of unheated and heated CHA, the heated CHA has higher crystallinity than the unheated CHA. It concluded that the heat

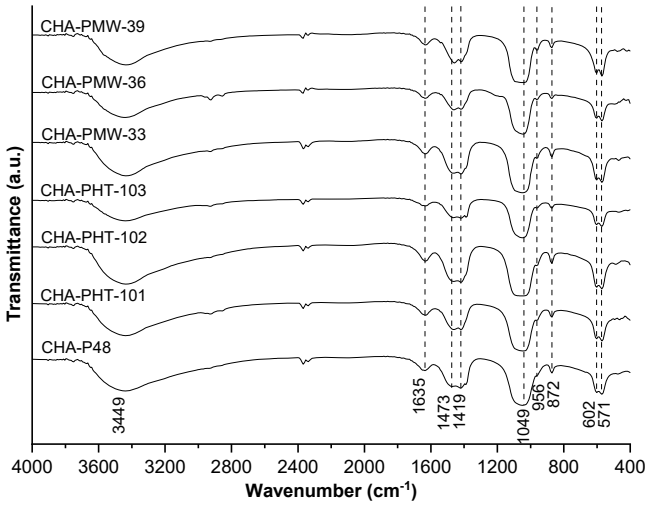

Fig 3. FTIR spectra of the CHA synthesized using hydrothermal-heated and microwave-heated precipitation methods with a time variation compared to the unheated CHA

Table 3. Crystal parameters of the synthesized materials

Materials	β_{002} (°)	Crystallinity (%)	Crystallite size (nm)
HA-PMW-39	0.280	63.300	28.290
CHA-P48	0.557	8.000	14.200
CHA-PHT-101	0.494	11.500	16.000
CHA-PHT-102	0.494	11.400	15.990
CHA-PHT-103	0.399	21.800	19.830
CHA-PMW-33	0.441	16.100	17.910
CHA-PMW-36	0.362	29.200	21.850
CHA-PMW-39	0.316	43.600	24.980

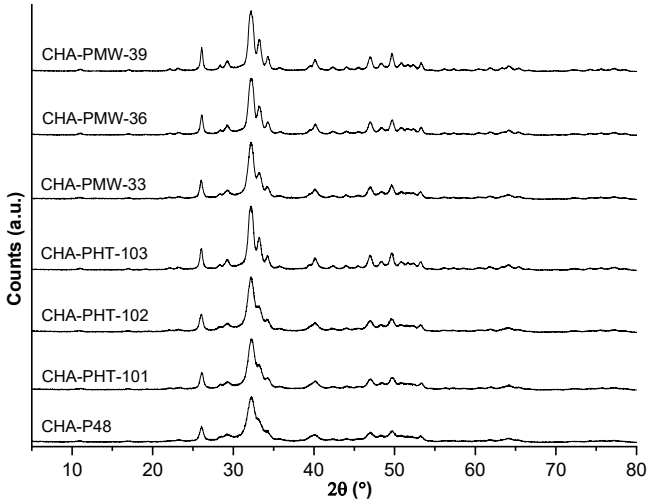

Fig 4. Diffractogram of CHA that was synthesized using hydrothermal-heated and microwave-heated precipitation methods with a time variation compared to the unheated CHA

treatment increases the crystallinity of CHA material. The same result was also obtained by Kalpana and Nagalakshmi [40]. The crystallite size and crystallinity of the HA were raised with the increase of the temperature in the precipitation method. Increasing the reaction temperature increases the nucleation rate, increasing grain growth and crystallinity [41-42].

The CHA materials were analyzed using the electron microscope. The SEM images in Fig. 5 showed the surface morphology of HA and CHA materials with or without heat treatment. The HA and CHA materials have an irregular, rough surface shape with rounded edges. The materials comprised Ca, P, and O atoms, as shown in Table 4, which are the main components of the HA constituent with a Ca/P ratio of 1.39–1.48. This result may differ from the Ca/P ratio of stoichiometric HA and is categorized as precipitated HA. Córdova-Udaeta et al. [43] stated that obtaining the stoichiometric HA using precipitation was difficult due to the supersaturation of ions in solution and the interstitial adsorption of water molecules in the HA crystal that led to the rapid formation of small HA crystallite, limiting the ideal PO_4^{3-} and OH^- arrangement for stoichiometric HA.

Table 4. The elemental analysis results using EDX

Materials	Element (%Mass)				Ca/P
	Ca	P	O	Na	
HA-PMW-39	27.40	15.20	48.74	-	1.39
CHA-P48	21.68	11.61	50.94	1.44	1.44
CHA-PHT-103	26.93	14.09	45.38	1.41	1.48
CHA-PMW-39	23.29	12.21	49.49	1.06	1.47

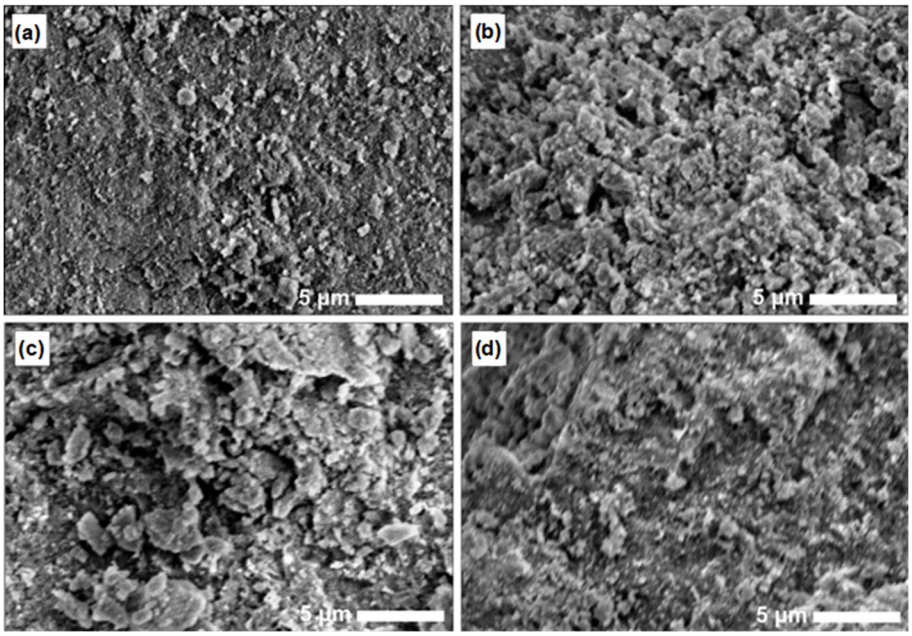

Fig 5. The SEM images of (a) HA-PMW-39, (b) CHA-P48, (c) CHA-PHT-103, and (d) CHA-PMW-39 materials

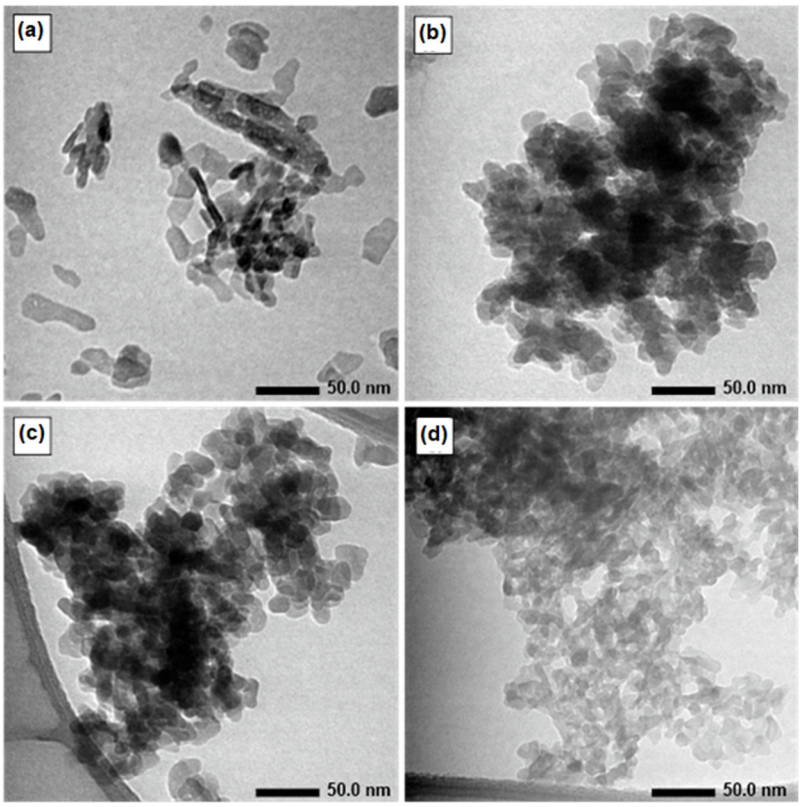

Fig 6. The TEM images of (a) HA-PMW-39, (b) CHA-P48, (c) CHA-PHT-103, and (d) CHA-PMW-39 materials

The carbon atoms were also found in the EDX results, which can come from the material or background, so they cannot be used as CHA material identifiers. The difference between HA and CHA can be seen by the appearance of Na atoms in the EDX results of CHA material due to using Na_2CO_3 as a carbonate source in the CHA synthesis. The Na atoms are incorporated in the HA lattice crystal to balance the charge on the HA crystal due to the substitution of PO_4^{3-} with CO_3^{2-}. The Na^+ (0.99 Å) has similar atomic radii as the Ca^{2+} (1.00 Å), so it can substitute the Ca^{2+} in the HA crystal lattice.

TEM images in Fig. 6 show that the HA and CHA materials synthesized using precipitation methods with or without heating treatment were agglomerates composed of nanosized particles. The HA had elongated square-shaped particles, while CHA had rounded square-shaped particles. There were no differences in the shape of CHA particles caused by different heat treatments, but there were differences in the particle size of the synthesized material. The average particle size of the material is obtained by measuring the length of the particles in the TEM image.

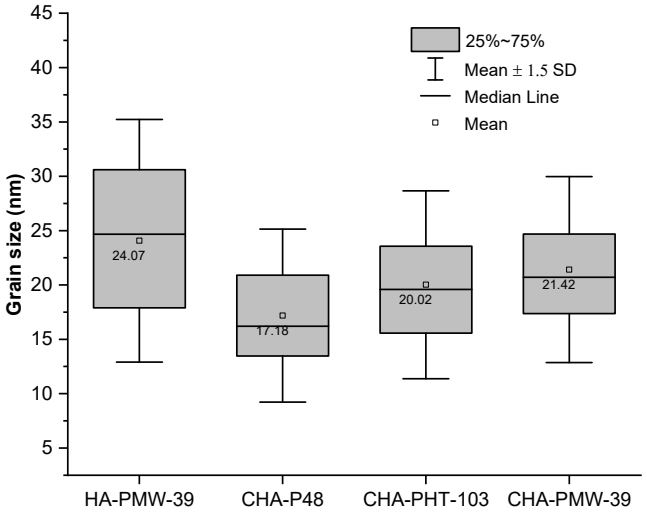

Fig 7. Grain size of CHA-P48, CHA-PHT-103, and CHA-PMW-39 materials

The results of particle size measurement are shown in Fig. 7. The HA material had the largest particle size. It proves that the carbonate ion in the CHA material can inhibit crystal growth, so the size of CHA particles is smaller than HA. The particle size of the materials was

also affected by the heat treatment. The CHA material without heating treatment had the smallest particle size among others. Then, the particle size increased as the heating treatment was applied. The particle size of the CHA with microwave heating treatment was larger than the CHA with hydrothermal heating treatment.

Then, the synthesized materials were immersed in the SBF solution to estimate their bioactivity. Kokubo and Takadama [34] found that the *in vivo* apatite forming on the material surface could be reproduced in SBF. SBF is a supersaturated solution that mimics the human body plasma. The prepared samples were immersed in SBF, and the apatite-like formation process and the material dissolution process were undergone. The dissolution process releases OH^- ion. Thus, the pH of the SBF solution increases. The apatite-like formation process will decrease the pH as the OH^- ions are required [36]. The pH of the SBF solution will depend on the dissolution rates and apatite-like formation processes. The system would have a higher pH if the dissolution rate were faster than the apatite-like formation. Conversely, if the rate of apatite-like layer formation were faster than the dissolution rates, the system would have a lower pH [36]. Fig. 8 shows that the graphs tend to decrease, revealing that the apatite-like layer formation rate was faster than the dissolution rate in HA and CHA materials. It concludes that both materials could accommodate the formation of the apatite-like layer on its surface. The change in pH of the SBF solution also indicated the chemical stability of the material [35]. The pH of the SBF varied from 7.24 and 7.38. This value was like the physiological pH value. Therefore, it can be concluded that the CHA and HA materials synthesized using the precipitation method with heat treatment were quite stable because the material did not change the pH of SBF far from the physiological pH value of 7.40 [35].

The results of measuring of energy used in heat involving process in the synthesis of CHA materials are presented in Table 5. The heat-involving processes were hydrothermal heating, microwave heating, and drying step. The hydrothermal heating used 750 W of electrical

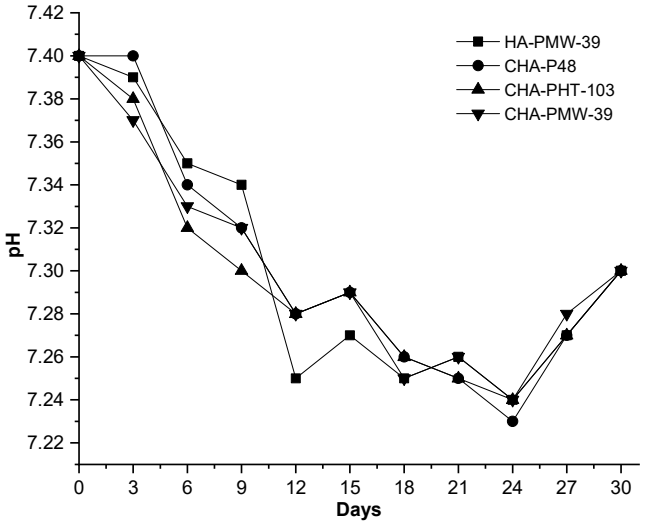

Fig 8. The changes in pH during materials immersion using SBF solution

Table 5. Electrical energy calculation of heat involving process in CHA synthesis

Material	Heat involving process	Time (h)	Energy used (kWh)	Total energy used (kWh)
CHA-P48	Drying	6	1.11	1.11
CHA-PHT-101	Hydrothermal	1	0.29	1.40
	Drying	6	1.11	
CHA-PHT-102	Hydrothermal	2	0.43	1.54
	Drying	6	1.11	
CHA-PHT-103	Hydrothermal	3	0.76	1.87
	Drying	6	1.11	
CHA-PMW-33	Microwave	0.05	0.01	1.12
	Drying	6	1.11	
CHA-PMW-36	Microwave	0.10	0.02	1.13
	Drying	6	1.11	
CHA-PMW-39	Microwave	0.15	0.02	1.13
	Drying	6	1.11	

power to heat the CHA synthesis process for 1, 2, and 3 h, while the microwave heating used 270 W of electrical power for 0.05, 0.10, and 0.15 h. Based on the diffractogram of the CHA material in Fig. 4 and the crystal parameter in Table 3, the CHA could be synthesized using the precipitation method without heating treatment. The synthesized CHA without heat treatment had low crystallinity and required a long time. The heat that was provided by hydrothermal and microwave heating was shown to increase the nucleation rate. Table 5 shows that the total energy calculation of CHA synthesis involving hydrothermal heating required higher electrical energy than microwave and no heating. Despite using more electrical energy, the crystallinity of CHA materials produced by hydrothermal heating was lower than that of microwave heating. Therefore, it was concluded that microwave heating was more effective than hydrothermal heating in providing heat to increase the nucleating rate, resulting in higher CHA crystallinity.

CONCLUSION

Hydrothermal and microwave heating can increase the efficiency of the CHA synthesis process. Synthesis of CHA using microwave and hydrothermal heating affected material characteristics, including crystallinity, crystallite size, and grain size. The material crystallinity, crystallite, and grain size increased due to the heat used. The heat treatment did not cause the formation of new crystalline phase changes in the functional group of the synthesized material. The duration of heat treatment also affected the crystallinity, crystallite size, and grain size. Microwave heating increased the crystallinity, crystallite size, and grain size higher than hydrothermal heating, though using lower energy than hydrothermal heating. This study concluded that microwave heating had better energy efficiency than hydrothermal heating in the CHA synthesis.

ACKNOWLEDGMENTS

The authors thank the Ministry of Research and Technology of the Republic of Indonesia for funding the research through the PMDSU scholarship (contract number 111/E4.1/AK.04.PT/2021) and the Biomaterials Division of Material Physics and Electronics Laboratory, Physics Department, Faculty of Natural Science and Mathematics, Universitas Gadjah Mada, for providing laboratory facilities.

AUTHOR CONTRIBUTIONS

Saifuddin Aziz, Harno Dwi Pranowo, Ika Dewi Ana, and Yusril Yusuf conceptualized the experiment. Saifuddin Aziz conducted the experiment. Harno Dwi Pranowo, Ika Dewi Ana, and Yusril Yusuf supervised the experiment. Harno Dwi Pranowo provided resources for the experiment. Harno Dwi Pranowo conducted the project administration. Saifuddin Aziz wrote and revised the manuscript. Harno Dwi Pranowo, Ika Dewi Ana, and Yusril Yusuf reviewed the manuscript. All authors agreed to the final version of this manuscript.

REFERENCES

[1] Xue, N., Ding, X., Huang, R., Jiang, R., Huang, H., Pan, X., Min, W., Chen, J., Duan, J.A., Liu, P., and Wang, Y., 2022, Bone tissue engineering in the treatment of bone defects, *Pharmaceuticals*, 15 (7), 879.

[2] Florencio-Silva, R., Sasso, G.R.S., Sasso-Cerri, E., Simões, M.J., and Cerri, P.S., 2015, Biology of bone tissue: Structure, function, and factors that influence bone cells, *Biomed Res. Int.*, 2015, 421746.

[3] Zhao, R., Yang, R., Cooper, P.R., Khurshid, Z., Shavandi, A., and Ratnayake, J., 2021, Bone grafts and substitutes in dentistry: A review of current trends and developments, *Molecules*, 26 (10), 3007.

[4] Haider, A., Haider, S., Han, S.S., and Kang, I.K., 2017, Recent advances in the synthesis, functionalization and biomedical applications of hydroxyapatite: A review, *RSC Adv.*, 7 (13), 7442–7458.

[5] Arokiasamy, P., Al Bakri Abdullah, M.M., Abd Rahim, S.Z., Luhar, S., Sandu, A.V., Jamil, N.H., and Nabiałek, M., 2022, Synthesis methods of hydroxyapatite from natural sources: A review, *Ceram. Int.*, 48 (11), 14959–14979.

[6] Firdaus Hussin, M.S., Abdullah, H.Z., Idris, M.I., and Abdul Wahap, M.A., 2022, Extraction of natural hydroxyapatite for biomedical applications—A review, *Heliyon*, 8 (8), e10356.

[7] Ana, I.D., Lestari, A., Lagarrigue, P., Soulie, J., Anggraeni, R., Maube-Bosc, F., Thouron, C., Duployer, B., Tenailleau, C., and Drouet, C., 2022, Safe-by-design antibacterial peroxide-substituted biomimetic apatites: Proof of concept in tropical dentistry, *J. Funct. Biomater.*, 13 (3), 144.

[8] Aziz, S., Ana, I.D., Yusuf, Y., and Pranowo, H.D., 2023, Synthesis of biocompatible silver-doped carbonate hydroxyapatite nanoparticles using microwave-assisted precipitation and *in vitro* studies for the prevention of peri-implantitis, *J. Funct. Biomater.*, 14 (7), 385.

[9] Herbanu, A., Ana, I.D., Ardhani, R., and Siswomihardjo, W., 2023, Fibrous PVA matrix containing strontium-substituted hydroxyapatite nanoparticles from golden apple snail (*Pomacea canaliculata* L.) shells for bone tissue engineering, *Bioengineering*, 10 (7), 844.

[10] Hayashi, K., Kishida, R., Tsuchiya, A., and Ishikawa, K., 2019, Honeycomb blocks composed of carbonate apatite, β-tricalcium phosphate, and hydroxyapatite for bone regeneration: Effects of composition on biological responses, *Mater. Today Bio*, 4, 100031.

[11] Kahil, K., Weiner, S., Addadi, L., and Gal, A., 2021, Ion pathways in biomineralization: Perspectives on uptake, transport, and deposition of calcium, carbonate, and phosphate, *J. Am. Chem. Soc.*, 143 (50), 21100–21112.

[12] Nakamura, M., Hiratai, R., Hentunen, T., Salonen, J., and Yamashita, K., 2016, Hydroxyapatite with high carbonate substitutions promotes osteoclast resorption through osteocyte-like cells, *ACS Biomater. Sci. Eng.*, 2 (2), 259–267.

[13] Januariyasa, I.K., Ana, I.D., and Yusuf, Y., 2020, Nanofibrous poly(vinyl alcohol)/chitosan contained carbonated hydroxyapatite nanoparticles scaffold for bone tissue engineering, *Mater. Sci. Eng., C*, 107, 110347.

[14] Yanny Marliana, B.I., Muhammad Syazwan, M.N, Ahmad-Fauzi, M.N., Balestri, W., and Reinwald, Y., 2021, Influence of ternary divalent cations (Mg^{2+}, Co^{2+}, Sr^{2+}) substitution on the physicochemical, mechanical and biological properties of carbonated hydroxyapatite scaffolds, *J. Aust. Ceram. Soc.*, 57 (5), 1499–1510.

[15] Permatasari, H.A., Sari, M., Aminatun, A., Suciati, T., Dahlan, K., and Yusuf, Y., 2021, Nano-carbonated hydroxyapatite precipitation from abalone shell (*Haliotis asinina*) waste as the bioceramics candidate for bone tissue engineering, *Nanomater. Nanotechnol.*, 11, 18479804211032851.

[16] Wang, X., Wan, C., Feng, X., Zhao, F., and Wang, H., 2021, *In vivo* and *in vitro* analyses of titanium-hydroxyapatite functionally graded material for dental implants, *Biomed Res. Int.*, 2021, 8859945.

[17] Deymier, A.C., Nair, A.K., Depalle, B., Qin, Z., Arcot, K., Drouet, C., Yoder, C.H., Buehler, M.J., Thomopoulos, S., Genin, G.M., and Pasteris, J.D., 2017, Protein-free formation of bone-like apatite: New insights into the key role of carbonation, *Biomaterials*, 127, 75–88.

[18] Safarzadeh, M., Chee, C.F., and Ramesh, S., 2022, Effect of carbonate content on the *in vitro* bioactivity of carbonated hydroxyapatite, *Ceram. Int.*, 48 (13), 18174–18179.

[19] Sadat-Shojai, M., Khorasani, M.T., Dinpanah-Khoshdargi, E., and Jamshidi, A., 2013, Synthesis methods for nanosized hydroxyapatite with diverse structures, *Acta Biomater.*, 9 (8), 7591–7621.

[20] Madupalli, H., Pavan, B., and Tecklenburg, M.M.J., 2017, Carbonate substitution in the mineral component of bone: Discriminating the structural changes, simultaneously imposed by carbonate in A and B sites of apatite, *J. Solid State Chem.*, 255, 27–35.

[21] Kolmas, J., Piotrowska, U., Kuras, M., and Kurek, E., 2017, Effect of carbonate substitution on physicochemical and biological properties of silver containing hydroxyapatites, *Mater. Sci. Eng., C*, 74, 124–130.

[22] Xue, C., Chen, Y., Huang, Y., and Zhu, P., 2015, Hydrothermal synthesis and biocompatibility study of highly crystalline carbonated hydroxyapatite nanorods, *Nanoscale Res. Lett.*, 10 (1), 316.

[23] Safarzadeh, M., Ramesh, S., Tan, C.Y., Chandran, H., Mohd Noor, A.F., Krishnasamy, S., and

Alengaram, U.J., 2019, Effect of multi-ions doping on the properties of carbonated hydroxyapatite bioceramic, *Ceram. Int.*, 45 (3), 3473–3477.

[24] Mohd Pu'ad, N.A.S., Abdul Haq, R.H., Mohd Noh, H., Abdullah, H.Z., Idris, M.I., and Lee, T.C., 2019, Synthesis method of hydroxyapatite: A review, *Mater. Today: Proc.*, 29, 233–239.

[25] Mobasherpour, I., Heshajin, M.S., Kazemzadeh, A., and Zakeri, M., 2007, Synthesis of nanocrystalline hydroxyapatite by using precipitation method, *J. Alloys Compd.*, 430 (1-2), 330–333.

[26] Correa-Piña, B.A., Gomez-Vazquez, O.M., Londoño-Restrepo, S.M., Zubieta-Otero, L.F., Millan-Malo, B.M., and Rodriguez-García, M.E., 2021, Synthesis and characterization of nano-hydroxyapatite added with magnesium obtained by wet chemical precipitation, *Prog. Nat. Sci.: Mater. Int.*, 31 (4), 575–582.

[27] Munir, M.U., Salman, S., Ihsan, A., and Elsaman, T., 2022, Synthesis, characterization, functionalization and bio-applications of hydroxyapatite nanomaterials: An overview, *Int. J. Nanomed.*, 17, 1903–1925.

[28] Núñez, D., Elgueta, E., Varaprasad, K., and Oyarzún, P., 2018, Hydroxyapatite nanocrystals synthesized from calcium rich bio-wastes, *Mater. Lett.*, 230, 64–68.

[29] Yelten-Yilmaz, A., and Yilmaz, S., 2018, Wet chemical precipitation synthesis of hydroxyapatite (HA) powders, *Ceram. Int.*, 44 (8), 9703–9710.

[30] Nowicki, D.A., Skakle, J.M.S., and Gibson, I.R., 2018, Nano-scale hydroxyapatite compositions for the utilization of CO_2 recovered using post-combustion carbon capture, *J. Mater. Chem. A*, 6 (13), 5367–5377.

[31] Hassan, M.N., Mahmoud, M.M., El-Fattah, A.A., and Kandil, S., 2016, Microwave-assisted preparation of nano-hydroxyapatite for bone substitutes, *Ceram. Int.*, 42 (3), 3725–3744.

[32] Saikiran, A., Vivekanand, M., Prahalad, M., Yuvan, S., and Rameshbabu, N., 2019, Microwave synthesis of Zn/Mg substituted and Zn/Mg-F co-substituted nanocrystalline hydroxyapatite, *Mater. Today: Proc.*, 27, 2355–2359.

[33] Singh, C., Khanna, V., and Singh, S., 2023, Sustainability of microwave heating in materials processing technologies, *Mater. Today: Proc.*, 73, 241–248.

[34] Kokubo, T., and Takadama, H., 2006, How useful is SBF in predicting *in vivo* bone bioactivity?, *Biomaterials*, 27 (15), 2907–2915.

[35] Ślósarczyk, A., Paszkiewicz, Z., and Zima, A., 2010, The effect of phosphate source on the sintering of carbonate substituted hydroxyapatite, *Ceram. Int.*, 36 (2), 577–582.

[36] Lijuan, X., Liuyun, J., Chengdong, X., and Lixin, J., 2014, Effect of different synthesis conditions on the microstructure, crystallinity and solubility of Mg-substituted hydroxyapatite nanopowder, *Adv. Powder Technol.*, 25 (3), 1142–1146.

[37] Benataya, K., Lakrat, M., Elansari, L.L., and Mejdoubi, E., 2020, Synthesis of B-type carbonated hydroxyapatite by a new dissolution-precipitation method, *Mater. Today: Proc.*, 31, S83–S88.

[38] Lafon, J.P., Champion, E., and Bernache-Assollant, D., 2008, Processing of AB-type carbonated hydroxyapatite $Ca_{10-x}(PO_4)_{6-x}(CO_3)_x(OH)_{2-x-2y}(CO_3)_y$ ceramics with controlled composition, *J. Eur. Ceram. Soc.*, 28 (1), 139–147.

[39] Kee, C.C., Ismail, H., and Mohd Noor, A.F., 2013, Effect of synthesis technique and carbonate content on the crystallinity and morphology of carbonated hydroxyapatite, *J. Mater. Sci. Technol.*, 29 (8), 761–764.

[40] Kalpana, M., and Nagalakshmi, R., 2023, Effect of reaction temperature and pH on structural and morphological properties of hydroxyapatite from precipitation method, *J. Indian Chem. Soc.*, 100 (4), 100947.

[41] Wasly, H.S., Abd El-Sadek, M.S., and Henini, M., 2018, Influence of reaction time and synthesis temperature on the physical properties of ZnO nanoparticles synthesized by the hydrothermal method, *Appl. Phys. A*, 124 (1), 76.

[42] Méndez-Lozano, N., Apátiga-Castro, M., Soto, K.M., Manzano-Ramírez, A., Zamora-Antuñano,

M., and Gonzalez-Gutierrez, C., 2022, Effect of temperature on crystallite size of hydroxyapatite powders obtained by wet precipitation process, *J. Saudi Chem. Soc.*, 26 (4), 101513.

[43] Córdova-Udaeta, M., Kim, Y., Yasukawa, K., Kato, Y., Fujita, T., and Dodbiba, G., 2021, Study on the synthesis of hydroxyapatite under highly alkaline conditions, *Ind. Eng. Chem. Res.*, 60 (11), 4385–4396.